This is the accepted manuscript version of the article

Fibre reinforced lightweight aggregates.

Bernhardt, M., Tellesbø, H., Justnes, H., & Wiik, K.

Citation for the published version (APA 6th)
Bernhardt, M., Tellesbø, H., Justnes, H., & Wiik, K. (2014). Fibre reinforced lightweight aggregates. *Journal of the European Ceramic Society, 34*(5), 1341-1351. doi:https://doi.org/10.1016/j.jeurceramsoc.2013.11.009

This is accepted manuscript version.
It may contain differences from the journal's pdf version.

This file was downloaded from SINTEFs Open Archive, the institutional repository at SINTEF
http://brage.bibsys.no/sintef

Fibre reinforced lightweight aggregates

Markus Bernhardt[a], Hilde Tellesbø[b], Harald Justnes[c], Kjell Wiik[a]

[a] Department of Materials Science and Engineering, Norwegian University of Science and Technology, NO-7491 Trondheim, Norway.

[b] Weber Leca Rælingen, NO-2008, Fjerdingby, Norway

[c] SINTEF, Building and Infrastructure, NO-7491, Trondheim, Norway

Department of Materials Science and Engineering, Norwegian University of Science and Technology, NO-7491 Trondheim, Norway.

Corresponding author: Kjell Wiik, Department of Materials Science and Engineering, Norwegian University of Science and Technology; Sem Sælands vei 12, 7491 Trondheim, Norway. Email: kjell.wiik@ntnu.no, phone: +4773594082

Abstract

Carbon steel fibre reinforced lightweight aggregates (LWA) were produced in a pilot scale rotary kiln. Narrow size fractions as well as not-sieved (as received) material were investigated according to European standards with a main focus on strength and density and compared to a reference material without fibres. Depending on the size of the pellets a fraction of the fibres oxidized during firing. A strength increase proportional to the amount of non-oxidized fibres within the pellet was observed. The crushing resistance for as received fibre reinforced pellets (bulk density 452 kg/m^3) was 3.0 MPa corresponding to an increase in strength of 140 %. The enhanced strength was also confirmed by the single pellet compression test.

*Keywords***:** Lightweight aggregate, fibre reinforcement, mechanical properties, crushing resistance, strength

1 Introduction

Lightweight aggregates (LWA) are commonly utilized as aggregate for lightweight concrete, insulation material for road constructions or in lightweight brick production [1-3]. Raw materials for LWA can be of artificial or natural origin [4-9]. Constant needs for stronger and lighter materials give the motivation of modifying and improving the properties of lightweight aggregates. LWA are highly porous, almost spherical particles that consist of a glassy matrix incorporating various types and amounts of crystalline inclusions. Consequently the material can be characterized as brittle and thus susceptible to catastrophic failure. A common way to improve the mechanical properties of brittle materials like ceramics or concrete is reinforcement with fibres. Various factors influence the success and degree of the fibre reinforcement: The difference in elastic-modulus between fibre and matrix as well as the strength-, distribution- and dimension of the fibres and the interfacial bond between fibre and matrix [10].

In the present investigation steel fibre reinforced lightweight expanded clay aggregates were produced and examined with a special focus on density and strength. A detailed determination of the strength of single LWA pellets requires the knowledge of the porosity, the density of the matrix phase and some geometrical factors of the sample as pointed out by Bernhardt et al [11]. All physical properties of the fibre containing LWA were compared to a reference material without fibres produced in the same way as the fibre reinforced samples. In this investigation the effect of fibre reinforcement on the strength of LWA-pellets is reported and possible toughening mechanisms are put forward and discussed.

2 Material and methods

2.1 Raw material and LWA manufacturing

Fibre containing lightweight aggregates were produced in a pilot scale rotary kiln. The raw material was clay blended with 1 wt.-% waste motor oil as expansion agent and carbon steel fibres of 1-2 mm length and approximately 30 µm diameter. Homogenization of the clay as well as the mixing of oil into the clay was performed by shaft mixers in an industrial production line at Saint-Gobain Weber in Norway. The fibres were supplied by the Swedish company “Ocklebo stål” and are made from milled steel wool. Mixing the fibres into the clay as well as the homogenisation and granulation of the material were executed in an eirich mixer. Dried clay powder was mixed with steel fibres before wet (approx. 20 % water content), oil containing clay and additional water (to reach sufficient plasticity to form pellets) was added. After homogenizing the mass was pelletized to granules of irregular size. Particles with diameters above 10 mm were removed before firing. The total fibre content of the material was 11.5 wt.-% (approx. 4.5 vol.-%) of the dry clay. LWA pellets without fibres were produced as a reference material using the same production procedure. The mineralogical and chemical composition of the raw clay was determined by an external research company called “IBU-tech advanced materials AG” using gravimetry, wet chemical quantification methods and X-ray diffraction.

The granulate material was fired in a continuous process in a direct heated (natural gas) rotary kiln of 10 m length and 0.3 m diameter. The approximate temperature distribution in the kiln is given in Fig. 1. Feeding of the kiln was executed by a dosing belt with a throughput of approximately 30 kg/h and the dwell time of the material in the kiln was about 30 min. Maximum burning temperatures varied from 1120°C for the reference material to 1090°C for the fibre containing material. The finished material was deposited on metal plates for initial cooling and thereafter put in metal drums and cooled to room temperature.

Figure 1

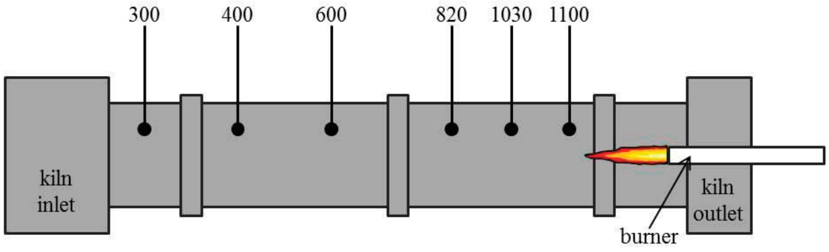

Caption Figure 1: Temperature profile in ºC of the rotary kiln. The dimensions of the kiln are 10 m length and 0.3 m diameter.

2.2 Material testing

The diameter after firing of the LWA pellets ranged from fine dust up to 15 mm for both the reference - and fibre containing material. The following tests were performed on as received (not sieved) material.

Oven dried particle density and water absorption after 24 h according to EN 1097-6 [12].

The loose bulk density (defined in [13]) by measuring the mass of 1 litre of bulk material.

Crushing resistance according to EN 13055-1 [14]; This standard test is executed with a sieving fraction of 4-22 mm.

Particle size distribution according to EN 933-1 [15] using the following mesh widths (given in mm): 31.5, 14, 12.5, 10, 8, 6.3, 4, 2, 1, 0.5;

Further tests were executed with the following size fractions (sieved): 1-2 mm, 2-4 mm, 4-6.3 mm, 6.3-8 mm, 8-10 mm and > 10 mm. Each sample consists of several individual pellets and the amount of tested pellets is given in Tab. 3. Samples are denoted as Ref- and Fib- where Ref- is the reference material without fibres and Fib- is the fibre containing material. The numbers represent the size fraction in mm (example: Fib-8-10 is the fibre containing material of the fraction 8-10 mm).

The average dry particle density, $\rho_{particle}$, of each sample was determined by sand pycnometry. Between 120 and 4700 individual pellets (depending on size) were put into a flask and covered with a known amount of fine sand to measure the volume. The particle density was calculated by dividing the mass of the material by the measured volume.

Helium pycnometry was used to determine the density of the matrix phase, ρ_{matrix}. Each density measurement was performed by milling a couple of pellets to a particle size < 36 micron and subsequently assessing the density in an AccuPyc 1330 helium pycnometer from micrometics. The average porosity, P, in per cent of each sample is calculated by Eq. 1.

$$P = 100 \cdot \left(1 - \frac{\rho_{particle}}{\rho_{matrix}} \right) \tag{1}$$

Single pellet strength was determined by uniaxial compression between 2 parallel rigid platens. The diameter of every single pellet was measured with a calliper before the granule was placed on the bottom plate of a press. Due to deviations from spherical geometry the diameter was measured between the highest and the lowest point when the pellet was lying in a stable position. Compression was performed with a constant speed of displacement of 2 mm per minute until a crack ruptured the pellet into at least two pieces. The applied load at failure, F_{crit}, of at least 50 pellets was recorded for each sample. The test equipment was a press made by “Instron ®” coupled to a load cell with a maximum capacity of 1 kN. The platen material was alumina. The solid strength, σ_{crit}, of each sample was calculated from the average load at failure, F_{crit}, the volume fraction of solid material, $\rho_{particle} / \rho_{matrix}$, and the average diameter, *D*, using Eq. 2.

$$\sigma_{crit} = \frac{F_{crit}}{D^2 \cdot \left(\rho_{particle} / \rho_{matrix}\right)^{2/3}} \tag{2}$$

Eq. 2 gives a strength value which is independent of the total porosity, *P* [11].

Prior to catastrophic failure, all pellets will suffer a certain “crumbling” (apparent plastic deformation) at the contact point between platens and pellet. The radius, a_c, of this “crumbled area” at the point of failure is important for the calculation of stress distribution and can be approximated from the average anvil displacement at failure, x, and the initial average radius of a sample, R, by Eq. 3 assuming a perfect sphere and equal damage/crumbling at the top and at the bottom [11].

$$a_c = \left(R^2 - (R - \frac{x}{2})^2\right)^{\frac{1}{2}} \tag{3}$$

Additionally to the single pellet compression test the crushing resistance, *C*, according to EN 13055-1 [14] was determined for the fractions 2-4 mm, 4-6.3 mm, 6.3-8 mm, and 8-10 mm for both the reference and the fibre containing material. The loose bulk density, ρ_{bulk}, of the same samples was determined prior to the crushing resistance test.

The chemical composition of the matrix phase of selected samples was assessed by X-ray florescence (XRF) analysis and normalized to 100 %. The bulk mineralogy of the same samples was determined by powder X-ray diffraction (XRD) using a D5000 (Siemens) with

Cu Kα radiation and operating parameters of 40 mA / 40 kV, step size 0.02°2 theta and 2.5 seconds step time.

The microstructure and chemical composition of the pellets were also investigated using a scanning electron microscope (SEM) from Hitatchi (C-3400N) combined with EDS (energy dispersive spectroscopy): Single pellets were cut in half, embedded in epoxy resin, polished and sputtered with carbon. Additionally the untreated fracture surface resulting from the single pellet compression test was investigated and the local chemistry of selected spots was also assessed by EDS.

A few selected samples were subjected to thermo gravimetric analysis (TGA) recording the mass gain in synthetic air at 1200°C. The samples where kept at 1200°C until constant mass. This method enabled a semi-quantitative analysis of the fibre content within a sample when assuming that the relative mass increase of fibre containing samples compared to reference samples were due to the oxidation of Fe to Fe_2O_3, Thus, the content of non-oxidized iron (Fe) in the fibre reinforced pellet could be assessed.

An overview of the whole production and investigation procedure is given in Fig. 2.

Figure 2

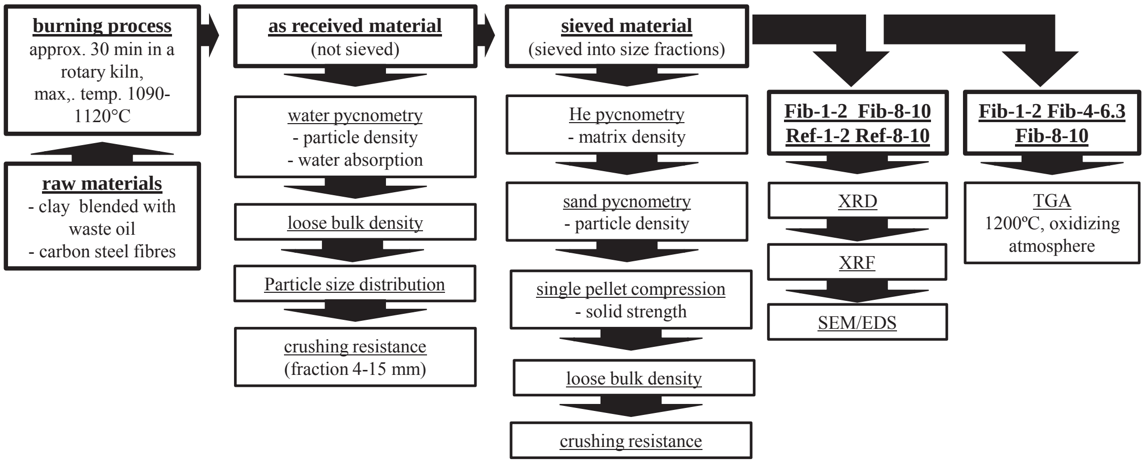
burning process
approx. 30 min in a rotary kiln, max,. temp. 1090-1120°C
raw materials
- clay blended with waste oil
- carbon steel fibres
as received material
(not sieved)
water pycnometry
- particle density
- water absorption
loose bulk density
Particle size distribution
crushing resistance
(fraction 4-15 mm)
sieved material
(sieved into size fractions)
He pycnometry
- matrix density
sand pycnometry
- particle density
single pellet compression
- solid strength
loose bulk density
crushing resistance
Fib-1-2 Fib-8-10
Ref-1-2 Ref-8-10
XRD
XRF
SEM/EDS
Fib-1-2 Fib-4-6.3
Fib-8-10
TGA
1200ºC, oxidizing atmosphere

Caption Fig. 2: Overview of the production process and the characterizations carried out on different types of samples.

3 Results

3.1 Raw material composition

The chemical and mineralogical composition of the raw clay is presented in Tab 1. The data is normalized to 100 %.

Table 1

mineralogical composition		chemical composition	
Quartz	17	SiO_2	59
Plagioclase	19	Al_2O_3	18
Orthoclase	6	Fe_2O_3	7
Amphibole	4	K_2O	4
Ilite/muscovite	40	MgO	3
Chlorite	10	CaO	2
Fe-Oxihydate	4	Na_2O	1
		TiO_2	1
		$LOI_{(1000°C)}$	5

Caption table 1: Mineralogical and chemical composition of the raw clay; the results are normalized to 100 % and are presented in wt.-%

3.2 Outer appearance of LWA pellets

Fig. 3 and Fig. 4 show LWA pellets with varying diameters both for the reference material and the fibre containing material. The reference material consists of a homogeneous, smooth shell and exhibits an almost spherical shape whereas the fibre containing material is less spherical and the surface is less smooth. Some oxidized carbon steel fibres are visible on the surface of fibre containing material in Fig. 4.

Figure 3

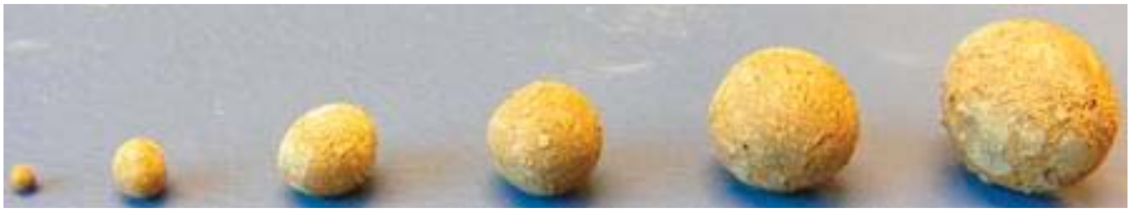

Caption Fig 3: Illustration of the reference material produced in a pilot-scale rotary kiln. Diameters range from 1.8 mm (left) up to 12 mm (right).

Figure 4

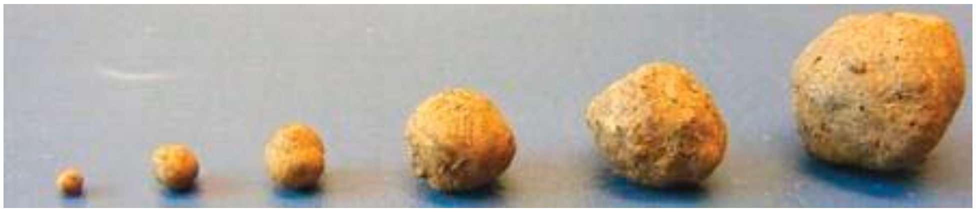

Caption Fig. 4: Illustration of carbon steel fibre containing LWA produced in a pilot-scale rotary kiln. Diameters range from 1.8 mm (left) up to 12 mm (right).

3.3 Properties of the as received (not sieved) material

Tab. 2 shows an overview of the properties of the whole fraction (as received from the kiln) for both the reference and fibre containing material. The increase in each value (property) between the reference and the fibre containing material is given in per cent.

The particle size distributions (PSD) for both materials are given in Fig. 5. The fibre containing material consists of a higher amount of small pellets (with diameters below 4 mm) compared to the reference. Generally diameters of both materials range from very fine particles (dust) to about 15 mm.

Table 2

	oven dried particle density [g/cm^3]	loose bulk density [kg/m^3]	water absorption after 24 h [wt.-%]	crushing resistance (pellets > 4 mm) [MPa]
Ref-as received	0.483	294	11.8	1.24
Fib-as received	0.721	452	13.5	2.97
increase [%]	49	54	14	140

Caption Table 2: Overview of the properties of the as received reference (Ref-) and fibre containing (Fib-) material

Figure 5

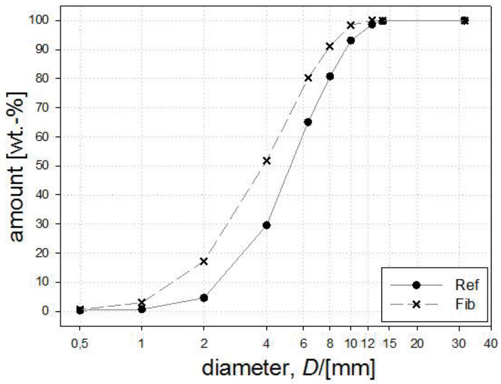

Caption Fig. 5: Particle size distribution of the reference and the fibre containing material

3.4 The effect of pellet size on density, porosity and strength

Tab. 3 shows an overview of the notations, size fractions and main properties of the sieved samples. In the following figures the value of a given property reported at a given sample diameter, *D*, is an average value resulting from at least 50 single pellets if not stated otherwise in chapter *2.2* The numerical values for the standard deviation are reported in Tab. 3 and also included as error bars in Fig. 9. However, error bars are not included in the remaining figures to enhance the readability. It should be emphasized that it was not possible to determine the standard deviation for all properties since some of them (i.e. density or porosity) are calculated from the average values of several pellets and not from each single pellet. Generally there is a large scatter in properties due to the heterogeneous nature of the material, therefore a large amount of samples were normally tested to obtain a representative average value.

Particle densities, $\rho_{particle}$, and loose bulk densities, ρ_{bulk}, are given in Fig. 6a)-b). The reference material shows a monotonously decrease with *D* for both type of densities. The samples Fib-1-2 to Fib-4-6.3 show a similar trend as the reference however less pronounced. At larger *D*'s (above 6.3 mm) both density values are more or less constant for the fibre containing material. Generally the density of the fibre containing material is higher than the density of the reference.

The matrix density, ρ_{matrix}, presented in Fig. 7 is generally higher for the fibre containing material than for the reference. Without the addition of fibres the matrix density is almost independent of *D* for all samples. This is to be expected given a homogeneous and constant composition of the raw material combined with a reproducible heat treatment. The matrix density for fibre reinforced materials is only independent of *D* in the low end and shows a rather pronounced increase with the diameter at *D*>4 mm. The general standard deviation of matrix density values of LWA produced from the given raw material could be approximated from the reference samples and was found to be about 0.06 g/cm^3.

The porosity, P, is given for all samples in Fig. 8. The reference material shows that LWA pellets typically exhibit an increasing porosity with increasing particle size. The same general trend is observed for the fibre containing material however with lower porosities and with the exception of the samples Fib-4-6.3 to Fib-8-10 which exhibit a plateau in the porosity trend.

Results of the single pellet compression test are presented in Fig. 9. The experimentally determined value for the average load at failure, F_{crit}, of each sample is plotted in dependency of the average pellet diameter, D. The error bars are given as plus-minus the standard deviation and show a significant scatter in F_{crit}. The force needed to crush the smallest fraction of pellets is almost the same for the reference- and the fibre containing material. Generally F_{crit} increases with D and the fibre containing pellets show a more pronounced increase than the reference.

The relative standard deviation (standard deviation in per cent of the average value) of the diameter, D, and the load at failure, F_{crit}, are given in Fig. 10. The deviation in D is between 6 % and 14 % for both type of materials at all diameters and the highest values are observed for the fractions 2-4 mm and 4-6.3 mm. The variation in the load at failure is generally quite high for all LWA pellets and average values for the relative standard deviation are 31 % for the reference material and 34 % for the fibre containing material, respectively.

Solid strength, σ_{crit} (Eq. 2), resulting from the single pellet compression test and the crushing resistance standard-test are presented in Fig. 11a)-b). The stress distribution within a pellet that is compressed between parallel platens can be influenced by the ratio between the radius of the contact area between platen and pellet, a_c, and the radius of the pellet, R [16, 17].

Stresses occurring along the load axis do not change significantly for 0.2 < a_c / R < 0.6 [16, 17] hence Eq. 2 provides reasonable values for the strength of the material within this range. a_c / R-values for different samples of the reference material range from 0.35 to 0.43 and from 0.34 to 0.48 for the fibre containing material. Consequently, a_c / R-values for all samples are within the required range.

The reference material exhibits a constant decrease in both types of strengths (σ_{crit} and *C*) with increasing diameter, *D* (cf. Fig 11a)-b)). The crushing resistance, *C*, of the fibre containing material follows the same trend but reaches higher absolute values. However, σ_{crit} for the fibre containing material remains almost constant with increasing diameter for *D*<8 mm. At larger diameter, *D*>8 mm, the solid strength, σ_{crit}, decreases with increasing *D*. The observed absolute values of σ_{crit} are again much higher for the fibre containing material than for the reference.

Table 3

sample	average diameter. *D* [mm]	sieving fraction [mm]	particle density. $\rho_{particle}$ [g/cm^3]	matrix density. ρ_{matrix} [g/cm^3]	porosity. *P* [%]	load at failure. F_{crit} [N]	solid strength σ_{crit} [MPa]	number of tested samples
Ref-1-2	1.9 (±0.12)	1-2	0.67	2.64 (±0.06)	75	14 (±5)	9.9	50
Ref-2-4	3.6 (±0.29)	2-4	0.58	2.61 (±0.06)	78	34 (±8)	7.1	50
Ref-4-6.3	5.3 (±0.72)	4-6.3	0.53	2.72 (±0.06)	80	57 (±17)	6.0	50
Ref-6.3-8	7.1 (±0.48)	6.3-8	0.49	2.68 (±0.06)	82	83 (±24)	5.0	50
Ref-8-10	8.8 (±0.66)	8-10	0.46	2.71 (±0.06)	83	101 (±26)	4.3	90
Ref>10	11.7 (±0.77)	> 10	0.39	2.70 (±0.06)	86	121 (±45)	3.2	50
Fib-1-2	1.8 (±0.12)	1-2	0.82	2.85 (±0.06)	71	15 (±4)	10.5	50
Fib-2-4	3.5 (±0.35)	2-4	0.74	2.84 (±0.06)	74	52 (±20)	10.2	50
Fib-4-6.3	5.3 (±0.49)	4-6.3	0.65	2.91 (±0.06)	78	109 (±40)	10.5	50
Fib-6.3-8	7.1 (±0.48)	6.3-8	0.67	3.00 (±0.06)	78	196 (±65)	10.6	50
Fib-8-10	8.8 (±0.54)	8-10	0.68	3.06 (±0.06)	78	282 (±106)	9.9	50
Fib>10	11.1 (±0.72)	> 10	0.62	3.13 (±0.06)	80	323 (±102)	7.7	50

Caption Tab 3: Overview of the notations, size fractions and main properties of the sieved samples of the reference (Ref-) – and fibre containing (Fib-) material.

Figure 6

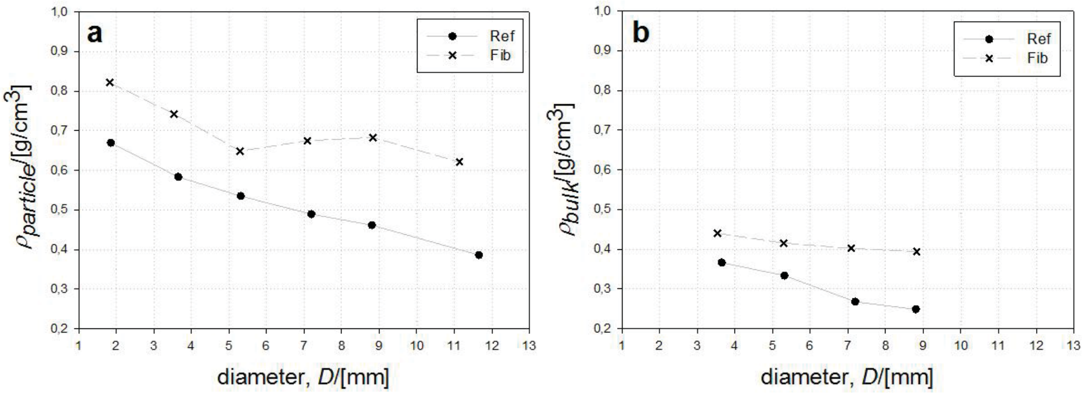

Caption Fig 6: Particle density (a) and loose bulk density (b) of the reference – and fibre containing material of different size fractions.

Figure 7

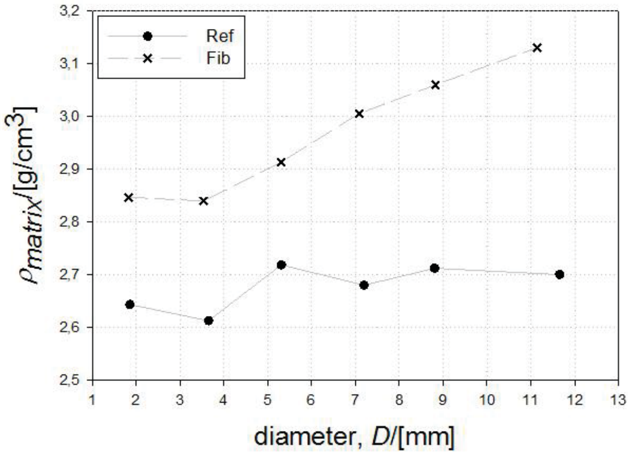

Caption Fig. 7: Matrix density of reference – and fibre containing material of different size fractions.

Figure 8

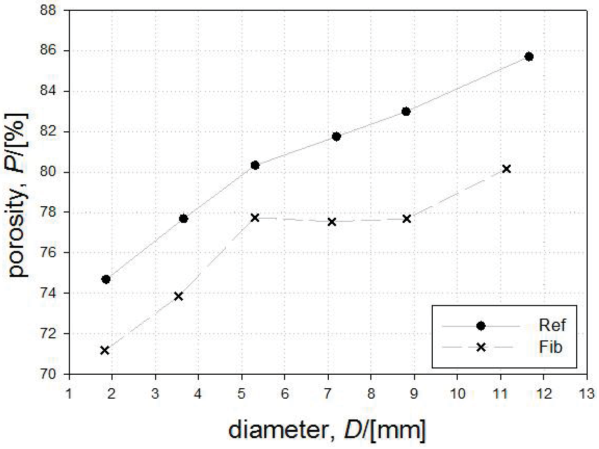

Caption Fig 8: Total porosity, *P*, of reference – and fibre containing material of different size fractions.

Figure 9

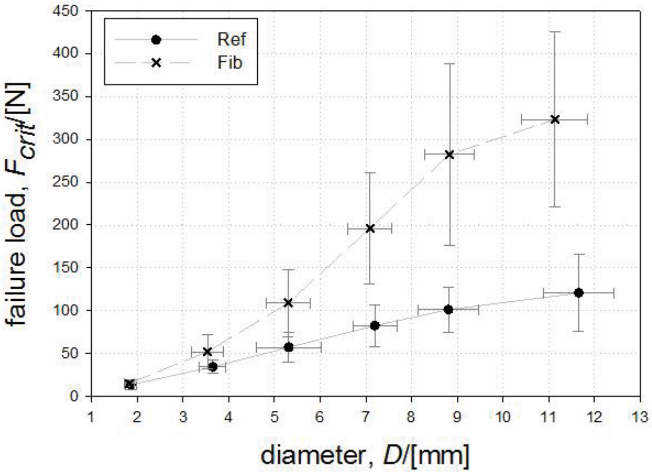

Caption Fig. 9: Load at failure obtained by single pellet compression of reference – and fibre containing material of different size fractions. The error bars are given as plus-minus the standard deviation of at least 50 samples.

Figure 10

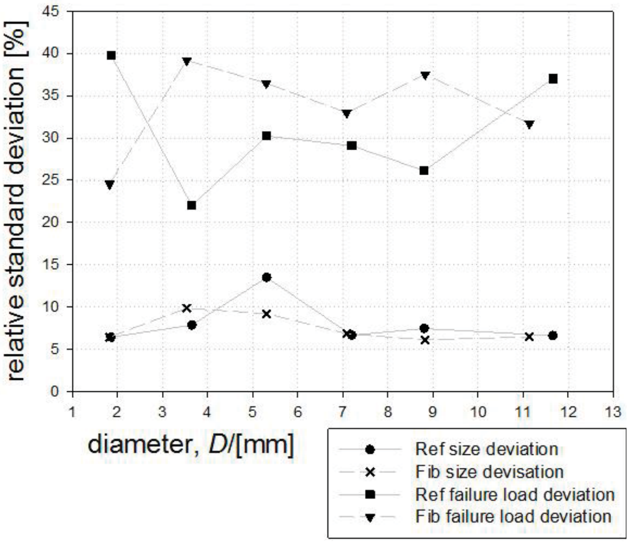

Caption Fig 10: Relative standard deviation (given in % of the average value) of the size and the failure load of reference – and fibre containing material of different size fractions.

Figure 11

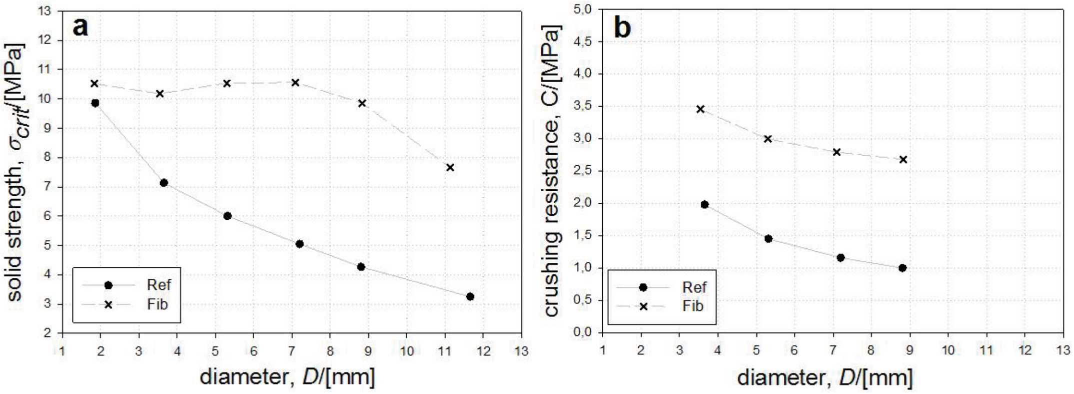

Caption Fig 11: Strength values resulting from single pellet compression (solid strength) (a) and crushing resistance (b) of reference – and fibre containing material of different size fractions.

3.5 Matrix composition

3.5.1 Chemical composition (XRF)

The chemical composition of the fractions 1-2 mm and 8-10 mm of both reference- and fibre containing material are given in Tab. 4. The reference samples do not show any large differences between the different size fractions while enhanced iron contents (given as Fe_2O_3 even though it is a sum of metallic iron and its oxides) were observed for the fibre containing samples and Fib-8-10 shows even a higher iron content than Fib-1-2.

Table 4

Sample	Ref-8-10	Fib-8-10	Ref-1-2	Fib-1-2
Fe_2O_3 (%)	7.7	24.9	7.8	20.3
TiO_2 (%)	0.9	0.7	0.9	0.8
CaO (%)	2.1	1.6	2.8	2.1
K_2O (%)	4.3	3.6	4.4	3.9
SiO_2 (%)	61.2	50.1	60.6	52.8
Al_2O_3 (%)	18.8	14.8	18.4	15.7
MgO (%)	3.1	2.6	3.1	2.7
Na_2O (%)	1.8	1.5	1.8	1.6
MnO (%)	0.1	0.2	0.1	0.2

Caption Table 4: XRF results for the fractions 1-2 mm and 8-10 mm of reference-and fibre containing material.

3.5.2 Mineralogical composition (XRD)

X-ray diffractograms of the same samples investigated by XRF are displayed in Fig. 12 and relative contents of phases that show a significant difference between fibre reinforced and reference samples (namely of iron (III) oxide and Fayalite (Fe_2SiO_4)) are given in Tab. 5. The matrix phase of the reference material consists of a high amount of glassy phase with the main crystalline inclusions being quartz, feldspar (mainly plagioclase) and hercynite. When adding carbon-steel fibres additional Fe_2O_3 was detected. Considering the peak size at 35.2° (2 Θ) the amount of Fe_2O_3 in Fib-1-2 seems higher than in Fib-8-10. Fayalite is observed in the fibre containing samples and appears to reach higher quantities in Fib-8-10 than in Fib-1-2 based on the peak size (cf. Tab. 5).

Figure 12

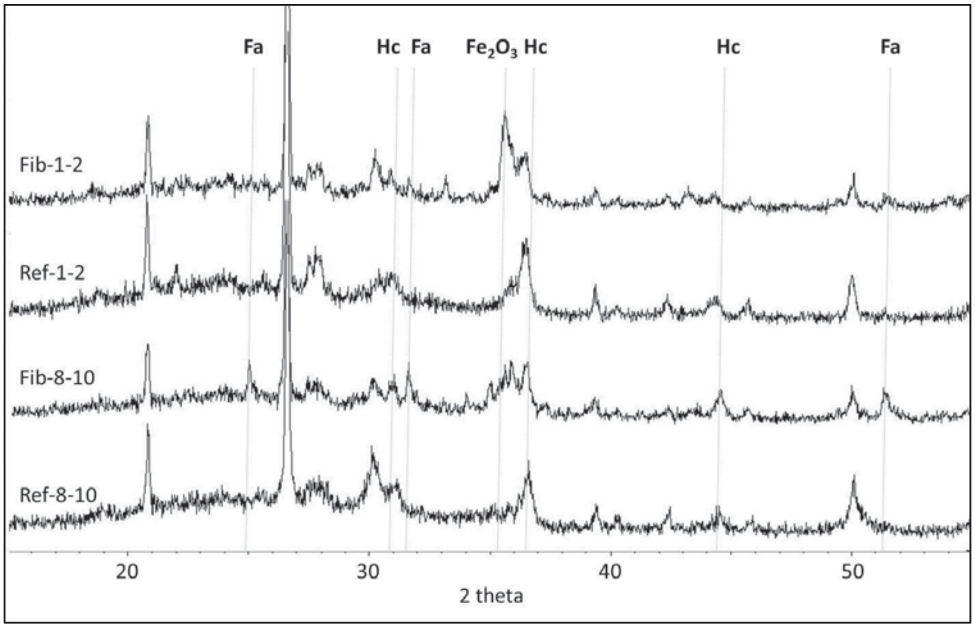

Caption Fig. 12: X-ray diffractograms of the fractions 1-2 mm and 8-10 mm of reference-and fibre containing material. Fa=Fayalite (Fe_2SiO_4), Hc=Hercynite ($Fe_2Al_2O_4$), the remaining peaks belong to quartz and feldspar.

Table 5

	Fe_2O_3	Fe_2SiO_4
Ref-1-2	-	-
Ref-8-10	-	-
Fib-1-2	XX	X
Fib-8-10	X	XX

Caption Tab. 5: Relative quantities of iron (III) oxide and Fayalite. Notation: – not detected; X small amounts and XX larger amounts.

3.6 Microstructure

Fig. 13 a)-b) show photographs from a reflected-light microscope picturing the porous microstructure of both types of LWA for the fraction 4-6.3 mm. The maximum pore size of the reference material is larger than for the fibre containing material, this was observed for all size fractions. It should also be noted that the total porosity is slightly higher for the reference material than for the fibre containing material (cf. Fig. 8).

Fig. 14 shows a BSE (back scattered electrons) image of the polished surface of one pellet of Fib-8-10. Fibres appear in bright white due to the higher density compared to the rest of the matrix phase. The fibres are distributed evenly throughout the whole pellet. EDS analysis revealed that in the vicinity of the surface of the pellet the fibres are oxidized as shown in Fig. 15 a) and the approximate chemical composition was found to be Fe_2O_3. However, towards the centre of the pellet the fibres consist of metallic iron due to reducing conditions in the inner pores. Fig. 15 b) pictures such a fibre and additionally reveals that the surface of the fibre has reacted with the surrounding matrix. BSE pictures of the sample Fib-1-2 are given in Fig. 16a)-b). In these rather small pellets no metallic iron was found indicating that all fibres were oxidized. Iron rich areas (light areas) were however found evenly distributed throughout the pellet supporting the assumption of a homogeneous fibre distribution. EDS analysis (Fig. 16 b)) revealed that even in the centre of these small pellets the fibres were completely oxidized (Fe_2O_3).

Figure 13 a + b:

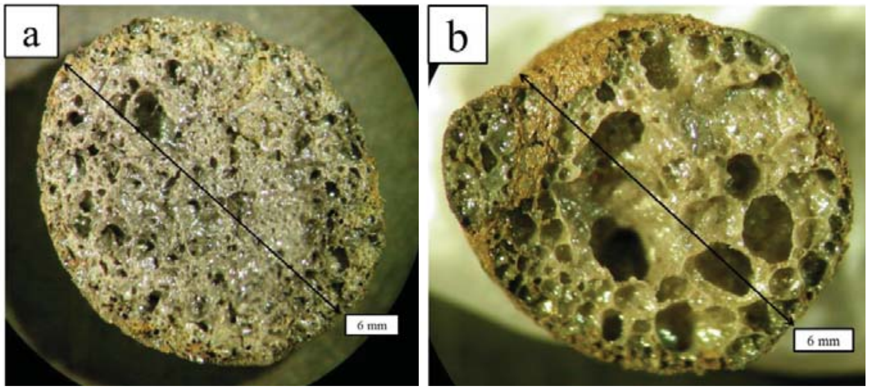

Caption Fig. 13: Porous micro structure of LWA pellets with 6 mm diameter containing carbon steel fibres (a) and without fibres (b) as observed form a reflected-light microscope.

Figure 14

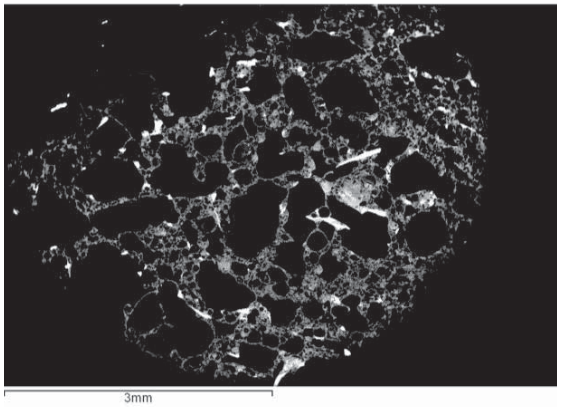

Caption Fig. 14: Backscattered electron image of a fibre containing LWA of the fraction 8-10 mm showing the distribution of the fibres (white) within the pellet.

Figure 15 a + b

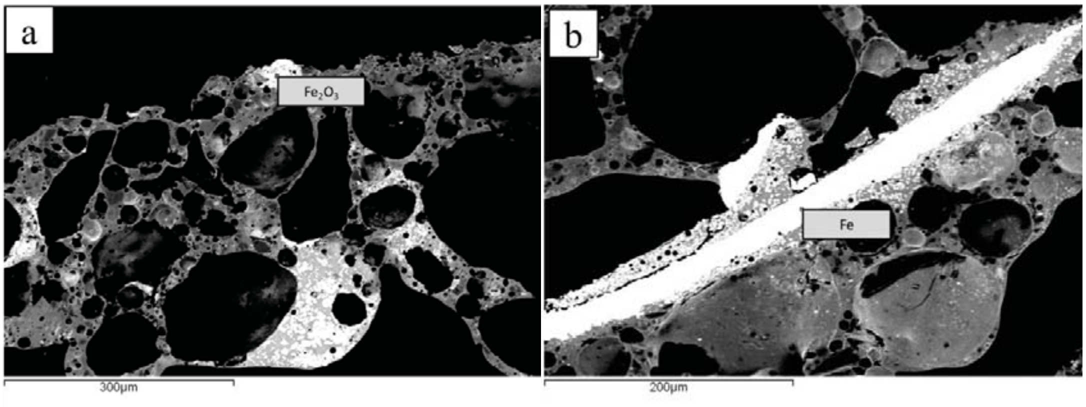
a
Fe$_2$O$_3$
300µm
b
Fe
200µm

Caption Fig 15: EDS investigations of a fibre close to the surface (a) and in the centre (b) of Fib-8-10 mm.

Figure 16 a + b

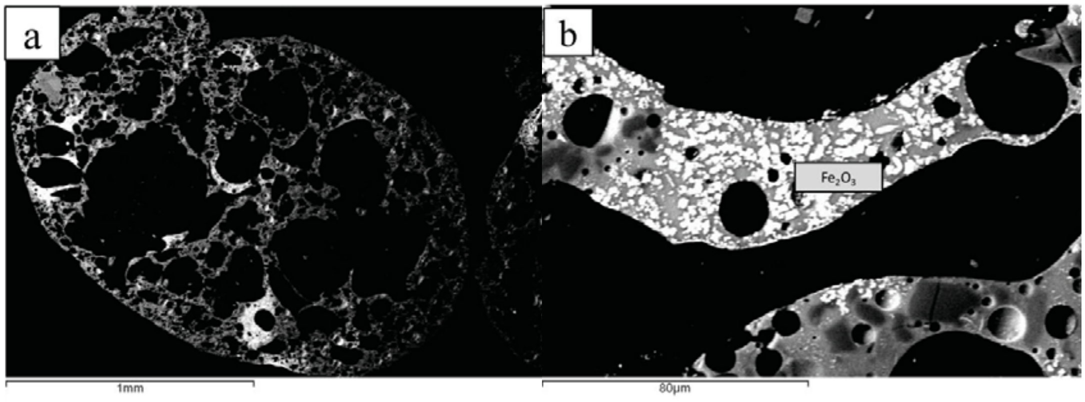
a
1mm
b
Fe$_2$O$_3$
80µm

Caption Fig 16: a: Backscattered electron image of Fib-1-2; b: EDS investigations of a oxidized fibre in the centre of the same pellet.

3.7 Thermo gravimetric analysis (TGA)

The weight gain of the samples Fib-1-2, Fib-4-6.3 and Fib-8-10 in oxidizing atmosphere at 1200°C is presented in Tab. 6. No weight increase was observed for the reference material and also Fib-1-2 shows the same behaviour. With increasing sample size (*D*), however, a larger weight increase was observed for fibre containing LWA.

Table 6

sample	weight increase (at 1200°C)[%]
Fib-1-2	0
Fib-4-6.3	1.35
Fib-8-10	2.94

Caption Table 6: Results of the TGA of different fractions of fibre containing LWA. Experiments were performed at 1200°C in oxidizing atmosphere

3.8 Fracture behaviour of fibre containing LWA

Fig. 17a) pictures the top of a pellet of sample Fib-8-10 directly after the single pellet compression test. The crumbled area resulting from the contact between platen and pellet is evident. Additionally, the crack dividing the pellet into two hemispheres is also observable. In contrast to the reference material, the fragments of fibre containing LWA pellets (in this case hemispheres) do not separate but stick together even after the platen has been removed subsequently to the strength test. After separating the two fragments by hand some fibres sticking out of the fracture plane are visible as shown in Figs. 17b)-c). The fracture surface of the same pellet is shown in Fig. 17d). It is difficult to identify the fibres since the contrast is low between fibre and matrix. However, the shiny metallic fibres become observable after grinding the fracture surface with SiC paper as shown in Fig. 17e).

BSE and SE images of the fracture surface are given in Fig. 18a)-d). A metallic fibre sticking out of the fracture surface is evident in Fig. 18b) and d) while another fibre covered with matrix phase at its surface is shown in Fig. 18a) and c).

Figure 17 a-e

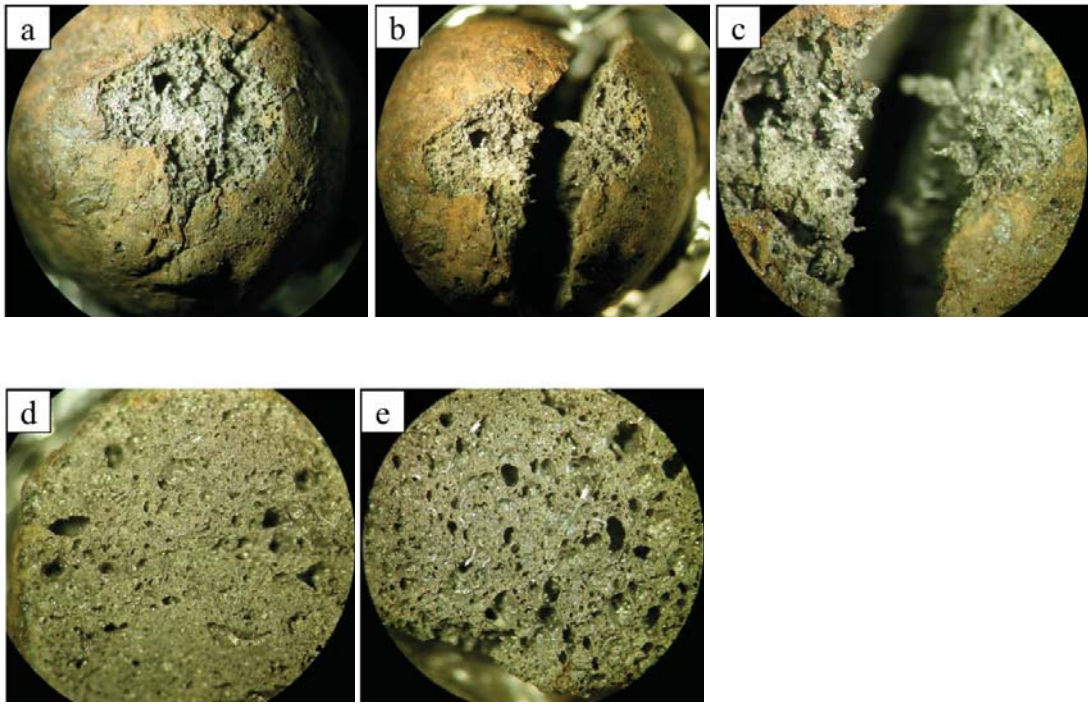

Caption Fig. 17: Photographs of a fibre containing LWA particle with 9 mm diameter after the single pellet compression test taken with a reflected light microscope: a: The top of the particle showing the crumbled area and the failure causing crack; b-c: Fibres sticking out of the fracture plain after separating the fragments from each other; d: Fracture surface; e: Fracture surface after grinding with SiC paper.

Figure 18 a-d

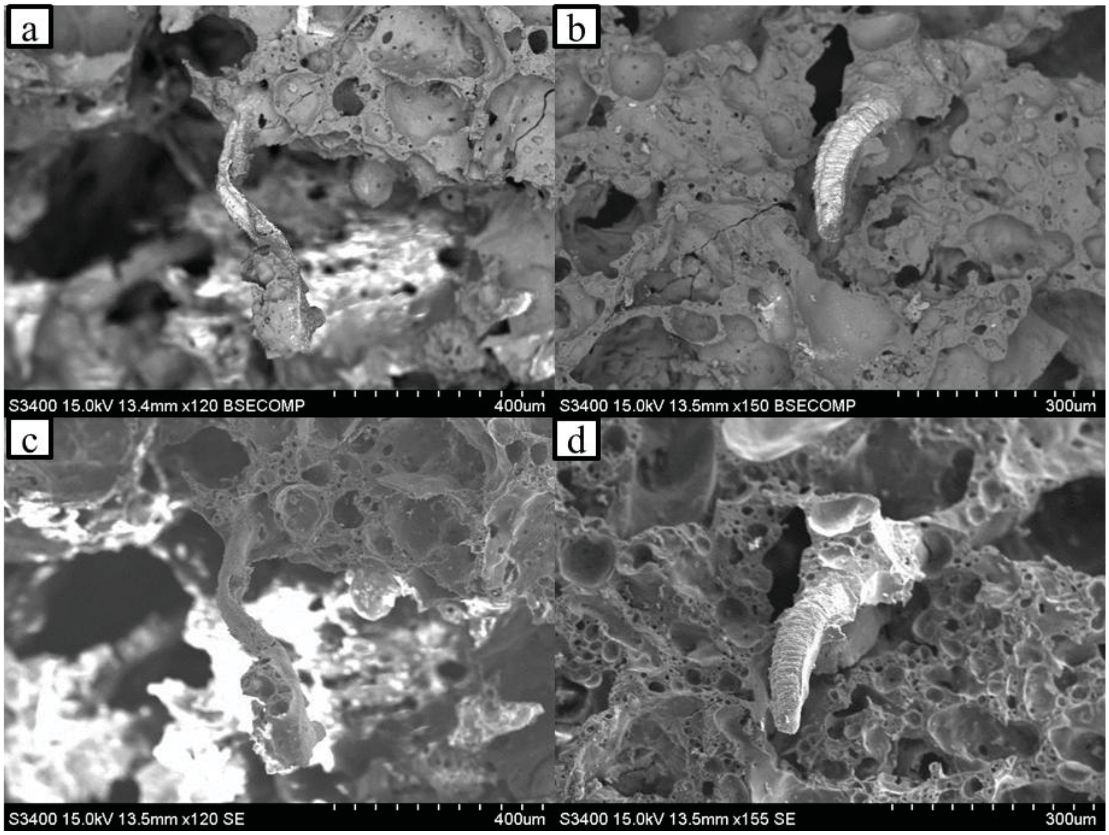
a
b
c
d
S3400 15.0kV 13.4mm x120 BSECOMP
400um
S3400 15.0kV 13.5mm x150 BSECOMP
300um
S3400 15.0kV 13.5mm x120 SE
400um
S3400 15.0kV 13.5mm x155 SE
300um

Caption Fig. 18: SE (a, b) and BSE (c, d) images of fibres within the untreated fracture surface of sample Fib-8-10 after the single pellet compression test.

4 Discussion

4.1 Properties of the as received material

The production of fibre containing expanded clay aggregates in a pilot scale rotary kiln was successful and the product exhibits clear differences in properties and appearance compared to the reference. The shape of fibre containing LWA pellets is less spherical which could be a disadvantage with respect to workability when utilized in concrete. According to Cheeseman at al. [18] a lightweight aggregate should feature a near-spherical shape to improve the properties of fresh concrete. Another disadvantage of the as-received fibre containing material is the increased bulk density and slightly higher water absorption (cf. Tab. 2) which influences the water-cement ratio when utilized in concrete. On the other hand the fibre containing material showed enhanced mechanical properties compared to the reference material.

4.2 Fibre content

It has been shown in section 3.4 that some material properties of fibre containing LWA develop differently with the sample size compared to the reference, this is most likely due to different quantities of non-oxidized fibres between the various fractions. Fig. 19 displays the approximate amount of metallic iron in different samples of fibre containing LWA as a function of the sample diameter. The values are semi quantitative and assessed by TGA. Fib-1-2 was found to contain no metallic iron and hence all the carbon steel fibres must have been oxidized during the production process. However, an increasing amount of metallic iron was confirmed with increasing pellet diameter, hence large pellets were able to suppress oxidation more effectively than small pellets. SEM/EDS and XRF analysis showed increased iron contents in both small - and large pellets of fibre containing LWA, confirming a homogeneous distribution of fibres in the raw material independent of the size of the pellets. SEM/EDS-analysis also confirmed complete fibre oxidation in small pellets while large pellets (> 4 mm) showed metallic iron in the centre and oxidized fibres in the vicinity of the pellet surface. The distribution of oxidized and non-oxidized fibres is probably due to the following: The expansion process of expanded clay aggregates is initiated by carbothermal reduction of the inherent content of iron oxide leading to highly reducing conditions (basically

CO(g)) inside the LWA pellet. The reducing atmosphere protects the fibres from oxidation at the elevated firing temperature. However, in the vicinity of the shell (surface of pellet) of large pellets and throughout the whole volume of small pellets the atmosphere is not sufficiently reducing (that is: short diffusion path for ambient oxygen) to prevent fibres from oxidation. The increased amount of iron oxide observed by XRD in fibre containing pellets is the result of these oxidized fibres.

The total amount of metallic iron in Fib-8-10 was found (TGA) to be approximately 7 wt.-% (2.5 vol.-%). This is a reasonable value considering that the nominal amount of added fibres was 11.5 wt.-% and the fact that a fraction of fibres oxidized during the firing process. Considering the results of SEM analysis it is evident that an increasing amount of non-oxidized metallic fibres is observed with increasing pellet diameter (Figs. 13-14).

Figure 19

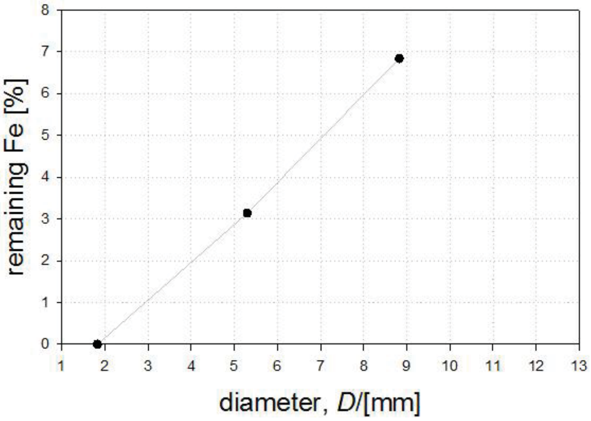

Caption Fig. 19: Approximate content of metallic iron found in the different fractions of fibre containing LWA after firing. Values are given in wt.-% and were obtained by TGA.

4.3 Relation between fibre content and physical properties of LWA

A summary of the effect of adding fibres to LWA is given in Fig. 20 whereas Fig. 20a) comprises values obtained from single pellets and Fig. 20b) comprises values obtained from bulk material. All properties are reported relative to the reference material (no fibres) and are based on data given in Figs. 6-8, 11. As previously discussed, the larger the diameter of a pellet the higher the amount of non-oxidized fibres consistent with the main trends given in Fig. 20a)-b): For small pellets all fibres will oxidize during the firing process and virtually no increase in solid strength is thus expected in accordance with Fig. 20a). The lower porosity and elevated matrix density for Fib-1-2 lead to an increased particle density of about 20 % compared to Ref-1-2 (cf. Fig 20a)), however without giving any increase in strength. On the other hand for the sample Fib-8-10 the amount of non-oxidized fibres was estimated to 7 wt.-% (2.5 vol.-%) and an increase in solid strength (indicating the strength of the matrix phase) of more than 130 % was observed. The crushing resistance of Fib-8-10 increased by 170 % compared to Ref-8-10 which is due to the enhanced solid strength and a higher packing density of the bulk material. The increased particle density (by 50 %) and bulk density (by 60 %) of Fib-8-10 compared to Ref-8-10 is caused by a lower total porosity and a larger matrix density (cf. Fig. 20a)-b)). A lower total porosity is due to the presence of fibres which will moderate the extent of expansion. The enhanced matrix density is also due to the presence of fibres simply because the steel fibres exhibit a significant higher density than the clay based matrix. Since the bulk density shows an even higher increase than the particle density (comparing Fib-8-10 and Ref-8-10) the packing density of Fib-8-10 in the one litre steel container must be higher than for Ref-8-10. That could be caused by a difference in particle size distribution or by the difference in particle shape described in section *3.2*. The same explanations given for the relative property trends of Fib-8-10 also apply for the samples Fib-2-4, Fib-4-6.3 and Fib-6.3-8.

The increase in solid strength of Fib>10 compared to Ref>10 is lower than expected from the increase in matrix density. A high matrix density usually indicates a high amount of non-oxidized fibres (ct. Figs. 7, 19) leading to a high solid strength. In case of Fib>10 the porosity is higher than in fibre containing samples with *D*<10 mm (cf. Fig. 8). It is possible that at high porosity levels some walls building up the porous interior of the pellet become too thin to be effectively reinforced by fibres. That would indicate that at a certain porosity threshold the reinforcing effect breaks down independently of the total fibre content.

Figure 20

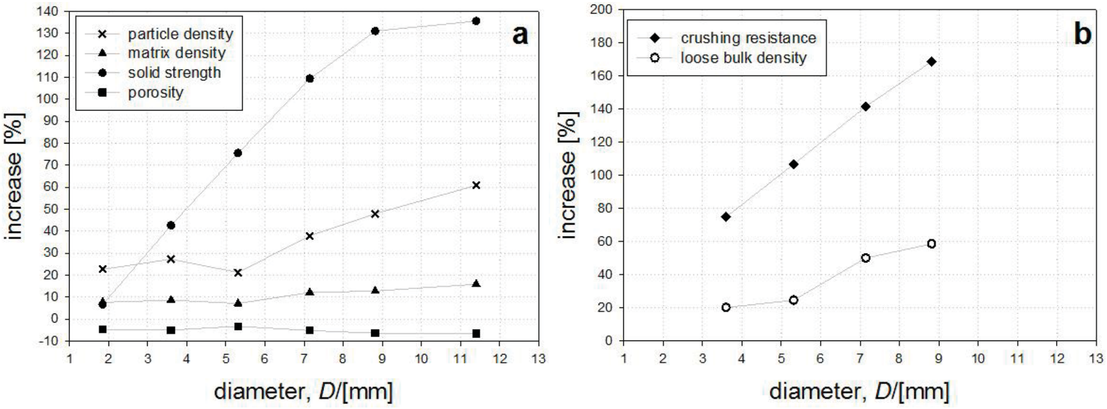

Caption Fig. 20: Development of the relative increase of various properties (caused by adding 11.5 % carbon steel fibres) with the sample diameter of LWA. a: Data obtained from single pellets; b: Data obtained from bulk material.

4.4 Possible toughening mechanisms for fibre reinforced LWA

Since the fibre containing LWA pellets change properties such as porosity, density and shape compared to reference pellets, the reason for the enhanced strength is not straight forward.

However, the given values for the solid strength are independent of the total porosity of a sample proving that the strength increase is not due to the lower porosity of the fibre containing samples. The extent of the strength increase for the fibre containing LWA pellets compared to the reference material is proportional to the amount of non-oxidized fibres most likely located at the centre of the pellet (cf. Fig. 19-20), supporting the assumption of strengthening by fibre reinforcement. In section 3.8 the fracture behaviour of fibre containing LWA was described and fibres sticking out of the fracture plane were observed in Fig. 17 b)-c) and Fig 18. Fibre pullout is therefore most likely the mechanism giving the best description of the observed toughening. In Fig. 15b) it is shown that the surface of the fibre partly has reacted with the surrounding matrix phase leading to a good adherence between fibre and matrix. However, fractured fibres were not observed at the fracture surface of the pellet, indicating that the fibre-matrix interface exhibit a strength appropriate to allow fibre pullout and hence reinforce the matrix [10, 19]. Moreover, the results from the XRD analysis showed that the fibre reinforced samples also contained fayalite (chemical composition Fe_2SiO_4) in contrast to the reference material. The formation of the fayalite takes place in the reaction zone between the fibre and the matrix-phase and may be the main responsible for appropriate bonding between fibre and matrix.

Besides fibre pullout another factor may also contribute to the observed strength increase of fibre containing LWA: The average pore size is smaller in the fibre containing LWA pellets than in the reference as shown in Fig. 13a)-b). A shift to smaller pore size may also enhance the strength, however no satisfactory documentation has yet been found in the literature reporting the effect of pore size distribution on the resulting strength.

Conclusions

Steel-fibre containing lightweight expanded clay aggregates were successfully produced in a pilot scale rotary kiln. The pellets were investigated with respect to mechanical properties and micro structure and compared to a reference material without fibres. During the firing process a fraction of the steel fibres oxidizes and the extent of oxidation was found to depend on the size of the pellet. Larger pellets include a certain volume of pores with highly reducing conditions protecting the fibres in the centre of the pellets from oxidation. At the surface of large pellets and throughout the whole volume of small pellets ambient oxygen diffuses into the aggregate and oxidizes the fibres. An increased solid strength and crushing resistance was observed for fibre containing LWA and the extent of the toughening was proportional to the amount of non-oxidized fibres within the pellet. The toughening mechanism was probably due to fibre pullout. Besides the enhanced mechanical properties the presence of fibres leads to lower porosities, a shift to smaller pore size, a higher matrix density and a change in chemical and mineralogical composition. Comparing the whole fraction of fibre containing LWA with the reference material an increase in crushing resistance of 140 % (corresponding to 3.0 MPa) was observed accompanied by a 54 % increase in bulk density (corresponding to 452 kg/m^3). For narrow fractions of LWA with high amounts of non-oxidized fibres even higher strength (crushing resistance) improvements of up to 170 % was obtained. Hence, steel-fibre reinforced LWA may prove useful in applications where high strength is required.

Acknowledgement

Financial support from Saint-Gobain-Weber and COIN (www.coinweb.no) as a part of SINTEF is gratefully acknowledged

References

1. Harding, M.A., Structural lightweight aggregate concrete. Aberdeen's Concrete Construction, 1995. 40(7).
2. Awwad, M.T., Hot mix asphalt using light weight aggregate concrete. Journal of Applied Sciences, 2007. 7(14): p. 1924-1929.
3. Sariisik, A. and G. Sariisik, New production process for insulation blocks composed of EPS and lightweight concrete containing pumice aggregate. Materials and Structures/Materiaux et Constructions, 2012. 45(9): p. 1345-1357.
4. Cheeseman, C.R. and G.S. Virdi, Properties and microstructure of lightweight aggregate produced from sintered sewage sludge ash. Resources, Conservation and Recycling, 2005. 45(1): p. 18-30.
5. González-Corrochano, B., et al., Microstructure and mineralogy of lightweight aggregates produced from washing aggregate sludge, fly ash and used motor oil. Cement and Concrete Composites, 2010. 32(9): p. 694-707.
6. Ducman, V., A. Mladenovič, and J.S. Šuput, Lightweight aggregate based on waste glass and its alkali-silica reactivity. Cement and Concrete Research, 2002. 32(2): p. 223-226.
7. Huang, S.C., et al., Production of lightweight aggregates from mining residues, heavy metal sludge, and incinerator fly ash. Journal of Hazardous Materials, 2007. 144(1-2): p. 52-58.
8. Swamy, R.N. and G.H. Lambert, The microstructure of Lytag aggregate. International Journal of Cement Composites and Lightweight Concrete, 1981. 3(4): p. 273-282.
9. Arioz, O., et al., A preliminary research on the properties of lightweight expanded clay aggregate. Journal of the Australian Ceramic Society, 2008. 44(1): p. 23-30.
10. Richerson, D.W., Modern Ceramic Engineering third ed 2006: Taylor and Francis group.

11. Bernhardt, M., et al., Mechanical properties of lightweight aggregates. Journal of the European Ceramic Society, submitted Feb. 2013 / accepted 21.04.2013.
12. CEN, EN 1097-6 Tests for mechanical and physical properties of aggregates - Part 6: Determination of particle density and water absorption, 2000.
13. CEN, EN 1097-3: Tests for mechanical and physical properties of aggregates - Part 3: Determination of loose bulk density and voids, 1998.
14. CEN, EN 13055-1 Lightweight aggregates - Part 1: Lightweight aggregates for concrete, mortar and grout, 2002.
15. CEN, EN 933-1 Tests for geometrical properties of aggregates - Part 1: Determination of particle size distribution - Sieving method, 2012.
16. Shipway, P.H. and I.M. Hutchings, Attrition of brittle spheres by fracture under compression and impact loading. Powder Technology, 1993. 76(1): p. 23-30.
17. Shipway, P.H. and I.M. Hutchings, Fracture of brittle spheres under compression and impact loading. Philosophical Magazine A, 1993. 67(6): p. 1389-1404.
18. Cheeseman, C.R., A. Makinde, and S. Bethanis, Properties of lightweight aggregate produced by rapid sintering of incinerator bottom ash. Resources, Conservation and Recycling, 2005. 43(2): p. 147-162.
19. Pemberton, S.R., et al., The fracture energy of metal fibre reinforced ceramic composites (MFCs). Composites Science and Technology, 2011. 71(3): p. 266-275.